Ocean Engineering 292 (2024) 116322

Contents lists available at ScienceDirect

Ocean Engineering

journal homepage: www.elsevier.com/locate/oceaneng

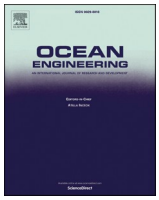

Multi-fidelity data-adaptive autonomous seakeeping

Michael D. Levine [a,*], Samuel J. Edwards [a], Dayne Howard [b], Kenneth Weems [a], Themistoklis P. Sapsis [b], Vladas Pipiras [c]

[a] Naval Surface Warfare Center, Carderock Division, 9500 MacArthur Boulevard, West Bethesda, MD, 20817, USA
[b] Massachusetts Institute of Technology, Department of Mechanical Engineering, 77 Massachusetts Avenue, Room 3-173, Cambridge, MA, 02139, USA
[c] University of North Carolina – Chapel Hill, Statistics & Operations Research, 318 Hanes Hall, CB #3260, Chapel Hill, NC, 27599-3260, USA

ARTICLE INFO

Handling Editor: Prof. A.I. Incecik

ABSTRACT

Safe operation of a ship in heavy weather and high sea states requires accounting for the risk of extreme ship motion responses in stochastic ocean waves. Excessive ship motions can lead to hazardous and unsafe conditions such as pure loss of stability, surf-riding and broaching. Mitigation of these risks can be performed through selection of ship speeds and headings for a given seaway, and avoiding conditions likely to lead to severe motions. To address this challenge, a robust, fast, data-adaptive model is a prospective enabling capability for onboard autonomous seakeeping. In this study, data-adaptive Long Short-Term Memory (LSTM) neural networks are investigated as part of a multi-fidelity approach incorporating Large Amplitude Program (LAMP), and a reduced-order model known as SimpleCode. An assessment of this multi-fidelity approach focuses on prediction of ship motion responses in waves. LSTM networks are trained and tested with LAMP simulations as a target, and SimpleCode simulations and wave time-series as inputs. LSTM networks are shown to improve the fidelity of SimpleCode seakeeping predictions relative to LAMP, while retaining the computational efficiency of a reduced-order model. Potential areas of application include unmanned and reduced-crew vessels, operator guidance for manned systems, and weather-informed ship route planning.

1. Introduction

To ensure the safe operation of a ship in heavy weather, operational guidance attempts to mitigate the risk of severe motions by selecting ship speeds and headings that minimize the probability of stability failures in the encountered wave conditions. This mitigation requires a reliable assessment of the seakeeping response of the hull with consideration of the ship loading conditions.

Due to the inherently random nature of the maritime environment, not every potential dangerous situation can be addressed and prevented at the ship design stage. The APL (American President Lines) China experienced parametric roll resonance during a stability accident in 1998 (France et al., 2003), which highlighted the need for ship-specific operational guidance. Consequently, parametric roll cannot always be prevented through reasonable design measures (Shin et al., 2004; Levadou and van't Veer, 2006). An important implication is that a ship cannot be made safe solely based on design. This real-world example highlights the importance of providing seakeeping guidance during ship operations.

Operational guidance has been a subject of on-going technical consideration. One of the first recommendations on avoidance of dangerous situations was published by the Maritime Safety Committee (MSC) of International Maritime Organization (IMO) MSC/Circ. 707 in 1995. Superseded by MSC/Circ. 1228 in 2007, it offered general recommendations without consideration of ship-specific behavior.

Recently, ship-specific operational guidance became a part of the IMO Second Generation Intact Stability Criteria, which addresses pure loss of stability, parametric roll, excessive accelerations, and surf-riding boarding modes of stability failure (MSC.1/Circ. 1627, IMO, 2020). Operational guidance is expected to be developed through state-of-the art modeling and simulations of ship hydrodynamics. The main intent of operational guidance is to inform the crew of specific features and behaviors of a ship, and aid in making informed decisions concerning ship operations in severe weather. The development of operational guidance for unmanned and reduced-crew vessels further expands the technical scope of the problem. Previous relevant studies have included decision support systems for operator guidance (Nielsen and Jensen, 2011; Nielsen et al., 2012), and ship routing (Dong et al., 2016).

* Corresponding author.
E-mail address: michael.d.levine@navy.mil (M.D. Levine).

https://doi.org/10.1016/j.oceaneng.2023.116322
Received 25 May 2023; Received in revised form 12 October 2023; Accepted 11 November 2023
Available online 23 December 2023
0029-8018/Published by Elsevier Ltd.

2. Multi-fidelity approach

To address the challenge of onboard autonomous seakeeping, a data-adaptive multi-fidelity approach may provide a plausible way for evaluating the expected ship motion responses for given seaways and ship loading conditions. Such a model could provide actionable information for autonomous seakeeping to improve safety of operation in realistic ocean environments.

While a reduced-order model such as SimpleCode (Weems and Wundrow, 2013) offers a significant advantage in processing speed, a fidelity gap still exists in the estimation of nonlinear responses as compared to predictions from a higher-fidelity but computationally intensive model such as Large Amplitude Motion Program (LAMP) (Shin et al., 2003).

In this paper, Long Short-Term Memory (LSTM) neural networks (Hochreiter and Schmidhuber, 1997) are considered as part of a multi-fidelity approach for the prediction of three degree of freedom (3-DOF) ship motion responses (heave, roll and pitch) to ocean waves. LSTM networks are trained and tested with LAMP simulations as a target, and SimpleCode simulations and wave time-series as inputs. In this study, LSTM networks are assessed in terms of improving the fidelity of SimpleCode seakeeping predictions relative to LAMP, while retaining the computational efficiency of a reduced-order model. The following sections provide the technical framework for consideration and initial assessment of this multi-fidelity approach.

2.1. High-fideliy hydrodynamic models

Physics-based seakeeping hydrodynamic models have been well established in multiple studies including by Lin and Yue (1990), Beck and Reed (2001), Shin et al. (2003), Reed and Beck (2016), and Belknap and Reed (2019). Most practical nonlinear seakeeping models are hybrid codes based on potential flow hydrodynamics, and also may include empirical coefficients based on model test data, high fidelity computational fluid dynamics (CFD), or engineering guidelines. While significantly faster than CFD, these hybrid models still require sufficient computational resources that preclude real-time applications. A typical solution to this problem is to generate a pre-computed lookup table (or database) of responses for specified wave and loading conditions. With this lookup table, the expected ship response is extracted corresponding to the encountered or forecasted sea conditions.

2.2. Problem of dimensionality

In development of a pre-computed look-up table, applicable seaway parameters available from weather forecasts include:

- o Significant wave height of primary system
- o Modal or mean-zero crossing period of primary system
- o Spread for primary system
- o Significant wave height of secondary system
- o Modal period or mean zero-crossing period of secondary system
- o Spread for secondary system
- o Propagation angle between primary and secondary systems

In addition to the environment, the generation of the lookup table requires information on ship loading conditions including:

- o Draft
- o Vertical location of the center of gravity
- o Trim

This resultant lookup table would have 10 dimensions with inclusion of these parameters. Rational grid design is essential, because it has direct impact on how many entries (or bins) are required for the lookup table. For example, a grid of 7 values for each of the 10 parameters would result in 282,475,249 (corresponding to 7^{10}) bins, which would be computationally prohibitive for time-domain simulations. Additionally, the problem of interpolation of a 10-dimensional parameter space is non-trivial. When developing pre-computed operational guidance, the number of parameters and values needs to be considered carefully. Ideally, the parameter space needs to cover realistic variations of the environmental and loading conditions potentially encountered.

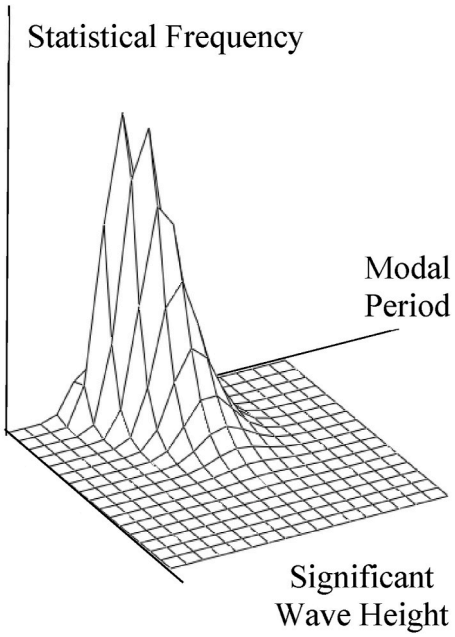

Fig. 1. Graphic representation of scatter table (IACS, 2001).

2.3. Correlation and approximation

The ocean environment is random and complex. Consequently, it is not realistic for a pre-computed database to capture every ocean condition potentially encountered. Accordingly, a computationally feasible approach is needed to estimate ship responses for a range of real-world conditions. A plausible way for addressing the dimensionality problem is based on the following assumptions:

- o Environmental parameters are dependent
- o Not all conditions are equally hazardous.

The scatter table from the International Association of Classification Societies (IACS) Recommendation 34 (IACS, 2001) is an example of dependence between the significant wave height and modal period as shown in Fig. 1.

This scatter table essentially is a histogram of the long-term distribution of significant wave height and modal period. Information on dependence can be extracted from the distribution and enable reduction in the number of required points. Alternatively, the scatter table can be characterized as a surface. The problem can then be posed as determining the minimum number of points to represent a surface.

Some of the parameters can be eliminated with conservative approximation. The spread of the short-crested waves can be estimated as an average, or waves can be assumed long-crested. The conservatism of the assumption of long-crested waves is that the dynamical system describing ship motion receives more concentrated energy as compared to short-crested seas.

Addressing a secondary system represents a separate problem for autonomous or reduced crew ships. When operational guidance is applied by a human operator, computations may be performed for one wave system. Once a two-wave-system seaway is forecasted, an

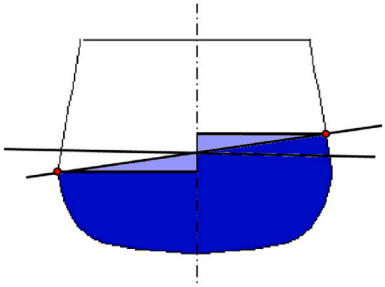

Fig. 2. Sample sectional volume calculation for ONR Topsides Series Tumblehome hull (Weems and Wundrow, 2013).

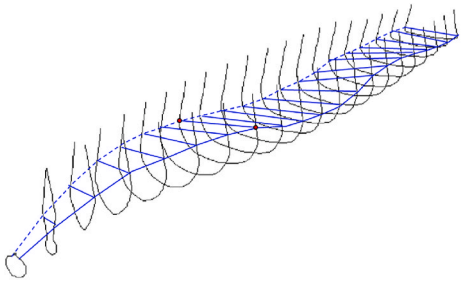

Fig. 3. Station/incident wave intersection points for the ONR Tumblehome hull in stern oblique seas (Weems and Wundrow, 2013).

experienced operator may determine which of the two systems is most hazardous and apply the appropriate guidance.

For an autonomous or reduced crew ship, decision-making can potentially employ artificial intelligence. A data-adaptive multi-fidelity approach may help address this problem.

2.4. Reduced-order model

The most straight forward approach is a Monte-Carlo style evaluation of motions for the observed or forecasted wave conditions; however, this requires a very fast and robust simulation system. A candidate for rapid simulations is based on the volume-based algorithm known as SimpleCode, which is described by Weems and Belenky (2018). SimpleCode can model the most important nonlinearities in ship motions in terms of body-nonlinear hydrostatic and Froude-Krylov forces. A resulting software implementation can support faster than real-time simulations (Weems and Belenky, 2018).

The main premise of SimpleCode is that by simplifying the local variation of wave pressure (i.e. Smith effect described in Bertram, 2011), the surface integral can be converted to a volume integral in the equations for hydrostatic and Froude-Krylov forces by employing Gauss theorem (equation 1 through 13 in Weems and Wundrow, 2013). As a result, the sectional hydrostatic and Froude-Krylov forces need only evaluate the instantaneous submerged volume and its geometric center. These calculations can be implemented to run very quickly with pre-computed Bonjean curves for each station plus a triangle correction reflecting the instantaneous roll relative to the wave in Fig. 2. The sectional calculation requires:

- o Finding an intersection of the flat waterline with sides
- o Interpolation of the pre-computed Bonjean curve in two points
- o Calculation of correction values for area and moments shown in light blue in Fig. 2

The complete instantaneous submerged volume and its center are computed by integration of the sectional values over the hull, which is illustrated in Fig. 3. These calculations run fast but do have a limitation.

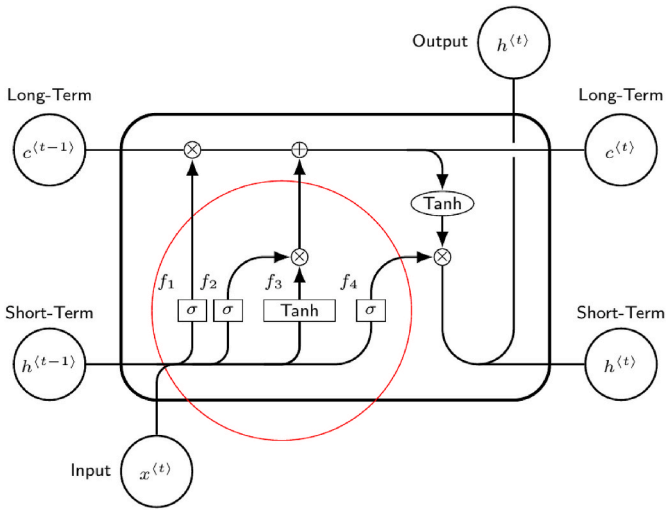

Fig. 4. Basic architecture of an LSTM cell.

The wave needs to be long enough in comparison with breadth to be reasonably approximated as a straight line across the beam. This is not usually a significant limitation in ship dynamics, because a wave comparable with ship breadth is not expected to cause an appreciable hazard.

The original intended use of SimpleCode was statistical validation of extrapolation methods (Smith, 2019), where the only requirement was qualitative validity. This qualitative validity was assured through reproduction of the inseparability of the hydrostatic and Froude-Krylov forces, which are understood to contribute significantly to the nonlinear characteristics of ship dynamics in waves.

As described in Weems and Belenky (2018), the SimpleCode approach is sufficient to produce a reasonable comparison with LAMP even with no diffraction and radiation forces. Diffraction and forces may be estimated in the SimpleCode via coefficients derived by regression techniques (Pipiras et al., 2021) with no significant impact on computational speed.

Another recent development has focused on maneuvering forces and motions in the horizontal plane. Weems et al. (2020) describe implementation of maneuvering hull forces based on regression from simplified Reynolds Averaged Navier-Stokes (RANS) simulations (double body – drift and rotating arm test). Employing regression for estimating hydrodynamic derivatives is a well-established technique that is applicable to SimpleCode.

A newer element that may be important for operational guidance is assessment of uncertainty. Weems et al. (2020) describe how uncertainty is evaluated for regression-based hydrodynamic derivatives that can be applied throughout the equations of motions.

As a result, recent developments may enable SimpleCode to be employed as a reduced-fidelity and quantitatively valid simulation tool, which combines volume-based calculations for hydrostatic and Froude-Krylov with regression-based diffraction, radiation and maneuvering forces. This reduced-fidelity model may include uncertainty quantification, making it a potentially viable approach for computationally efficient predictions of six degree of freedom (6-DOF) motion responses of a hull form for a defined set of wave conditions.

2.5. Long Short-Term Memory (LSTM) networks

An LSTM network (Hochreiter and Schmidhuber, 1997) is a type of recurrent neural network, which incorporates both short and long-term effects based on data-adaptive learning for estimation of a system, function, or process. The architecture of an LSTM cell including inputs, outputs, and short and long-term memory components is shown in

Fig. 4.

Inside the cell, the functions labeled (f_1, f_2, f_3, f_4) are representative of component-based operations. *Sigma* (σ) is the sigmoid activation function, and *tanh* is the hyperbolic tangent activation. The size of the weight and bias matrices in the LSTM layer defines the size or dimensionality of the hidden and cell states.

The following equations show the compact form of the operations inside of the cell.

$$f_1 = \sigma\left(W_{f1} \bullet x^{\langle t \rangle} + U_{f1} \bullet h^{\langle t-1 \rangle} + b_{f1}\right) \tag{1}$$

$$f_2 = \sigma\left(W_{f2} \bullet x^{\langle t \rangle} + U_{f2} \bullet h^{\langle t-1 \rangle} + b_{f2}\right) \tag{2}$$

$$f_3 = tanh\left(W_{f3} \bullet x^{\langle t \rangle} + U_{f3} \bullet h^{\langle t-1 \rangle} + b_{f3}\right) \tag{3}$$

$$f_4 = \sigma\left(W_{f4} \bullet x^{\langle t \rangle} + U_{f4} \bullet h^{\langle t-1 \rangle} + b_{f4}\right) \tag{4}$$

$$c_t = f_1 \circ c^{\langle t-1 \rangle} + f_2 \circ f_3 \tag{5}$$

$$h_t = f_4 \circ tanh(c^{\langle t \rangle}) \tag{6}$$

Weights are represented by (W, U), biases (b), and Hadamard product $(\circ)$. Based on the training of the neural network, each of the weights and biases are "learned". The hidden state (h_t) and cell state (c_t) act as "memory", and change over time.

Function (f_1) is the "forget gate", which controls the parts of the long-term state that are deleted. Function (f_3) represents the input gate, which controls the information from (f_2) that is added to the long-term state. Function (f_4) controls the output gate, which determines the output of the long-term state.

By constructing layers of cells, the LSTM network is capable of forecasting a desired response to a provided input. An LSTM network effectively maps the input time-series to the desired output time-series or targets. Increasing the number of layers can enable the network to model more complex interactions or behaviors.

The training process of the LSTM network is dependent on the selection of hyperparameters, which impact the accuracy and time-efficiency of the network. The hyperparameters consist of the number of inputs, number of network layers, training data sequence length, time resolution of the input time-series, hidden state size, bi-directionality, and dropout probability. The length of the training data sequences is equivalent to the number of samples of the input time-series.

Time resolution is based on uniform resampling of the input and target time-series. Through resampling, each time-series is reconfigured into a matrix of size $[N/\tau, \tau]$; where, N is the original time-series length, and τ is the time resolution factor. If N is not divisible by τ, then the time-series is reduced in length to the closest multiple of τ.

The network includes layers of LSTM cells that contain hidden states. The hidden state size is the number of parameters (h), which affects the number of weights in an LSTM unit. Size of the weight vectors are $W \in R^{hxd}$ and $U \in R^{hxd}$ for hidden state size (h), and number of input time-series channels (d). Increasing the hidden state size and number of LSTM layers can improve the ability of the network to recognize patterns with greater complexity, but can also result in model over-fitting and increased training time.

Bi-directional networks consider the relationship between input and target time-series in both forward and backward directions in time. Incorporation of bi-directionality generally increases the number of patterns that can be recognized, but results in longer training times.

Dropout is a regularization method where individual units and corresponding connections are removed temporarily from the network on a random basis of probability $(1 - p)$. During training, random removal helps to reduce over-fitting. During testing, the units and connections are restored, with weights (w) then becoming the expected weights $(p \bullet w)$.

Recent applications of LSTM networks to ship hydrodynamics include implementation with critical wave groups and CFD for predicting of extreme events of free-running vessels (Silva et al., 2022), estimation of nonlinear roll in response to irregular waves (Xu et al., 2021), and mooring line tension in response to input ship motion time-series (Qiao et al., 2021).

3. Methods and models for seakeeping guidance

3.1. Overview

Operational guidance is essentially a set of motion response predictions for a range of potential ship speeds and headings in encountered wave conditions. Based on application of prescribed limits to ship motions, recommended safe speeds and headings can be generated for a given seaway.

The validity of this guidance depends on the accuracy and reliability of the motion response predictions, which are based on the quantitative validity of the simulation system employed. In this work, validity is provided via a multi-fidelity approach. The approximations applied in the reduced fidelity models are generated by higher fidelity simulation tools that appear to be quantitatively valid (Lin and Yue, 1990; Smith, 2019).

Application of this multi-fidelity approach requires further steps in the development of automated operational guidance, which includes running additional simulations and verifications. The number and complexity of these steps depends on the completeness of the reduced-order model. Current and prospective methodologies and models for the development of operational guidance are presented in the following sections.

3.2. Reduced-order model

A 3-DOF reduced-order model includes vertical motions in terms of heave, roll, and pitch. Following the requirements of the Second Generation Intact Stability Criteria MSC.1/Circ. 1627 (IMO, 2020), this model can handle excessive accelerations and parametric roll failure modes. A procedure is envisioned with the following steps:

1. Estimation of damping based on the updated International Towing Tank Conference (ITTC, 2021) Recommended Procedure 7.5-02-07-04.5.
2. If roll damping is based on model testing or RANS simulations where the wave component is included inherently, then additional roll damping calibration is applied following Section 3.3.2.2 of MSC.1/Circ. 1627 (IMO, 2020), and further details in section 6 of Belenky et al. (2011).
3. Estimation of diffraction and radiation forces for heave, roll, and pitch via a series of potential flow simulations and regression.
4. Selection of several of the most probable sea states, and potential flow simulation with the damping calibration results.
5. A reduced-order simulation tool is then run to verify consistency.

3.3. Generation of wave data

Once a weather forecast is received, the expected seaway conditions are known, and elevations ζ_w of irregular waves can be computed based on the Longuet-Higgins (1984) model. For the case of long-crested waves:

$$\zeta_w(x,t) = \sum_{i=1}^{N} a_i \cos\left(k_i x - \omega_i t + \varphi_{0i}\right) \tag{7}$$

x is longitudinal coordinate (in meters), t is time (seconds), a_i is amplitude (meters), k_i is wave number or spatial frequency (radians per meter), ω_i is temporal frequency (radians per second), and φ_{0i} is random initial phase (radians). A uniform distribution of 0 to 2π is assumed for

the random initial phase. Wave number k_i is computed from frequency with the Airy wave dispersion relationship, where g is gravity acceleration:

$$k_i = \frac{\omega_i^2}{g} \tag{8}$$

Amplitudes a_i are computed from the spectral density, where $\Delta\omega$ is frequency increment:

$$a_i = 2\sqrt{s(\omega_i)\Delta\omega} \tag{9}$$

$s(\omega_i)$ is the resultant spectral density:

$$s(\omega_i) = s_{\mathrm{PWS}}(\omega_i) + s_{\mathrm{SWS}}(\omega_i) \tag{10}$$

In this above equation, s_{PWS} is the spectral density of the primary wave system (typically wind waves), and s_{SWS} is the spectral density of the secondary wave system (swell).

The capability to account for a secondary wave system by a precomputed lookup table is challenging because of the dimensionality problem. Secondary waves can be potentially addressed as part of a data-adaptive reduced-order model based on most probable encountered bi-directional sea conditions from historical weather data.

3.4. Speed-heading polar plot

Conventionally, operational guidance for a given seaway and loading condition is generated and displayed as a speed-heading polar plot, which is defined by combinations of ordered speeds and wave headings (relative to the primary wave system). A set of motion parameters is computed for each ordered ship speed-heading combination (node).

For a given node, if all the relevant ship motion parameters are less than established respective thresholds, then the node is designated as safe. If one or more of the parameters exceed a threshold, then the risk index is designated as unsafe.

Once the polar plot is computed, automated seakeeping guidance can be applied as part of ship route planning, which directs an autopilot to avoid certain headings, and imposes restrictions on the speed of the vessel.

The choice of the motion parameters is a somewhat open issue. American Bureau of Shipping (ABS, 2019) applies maximum value of roll angle observed for a certain time duration of simulation. MSC.1/Circ. 1627 (IMO, 2020) recommends two alternatives:

1. Upper boundary of the confidence interval as a failure rate estimate (for probabilistic guidance, section 4.5.4 of MSC.1/Circ. 1627).
2. Two times the 3-hour maximum roll or lateral acceleration (for deterministic guidance section 4.5.5 of MSC.1/Circ. 1627, IMO, 2020).

3.5. Single significant amplitude (SSA)

In seakeeping studies, response levels are typically computed as single significant amplitudes. SSA is an estimate of the largest one-third of observed amplitudes of motion or acceleration process. The amplitudes of a stochastic process are defined as absolute values of mean-crossing peaks. If the process is Gaussian:

$$\widehat{SSA} = 2 \bullet \sqrt{\widehat{V}_x} \tag{11}$$

where $\widehat{V}_x$ is a variance estimate of the process and a symbol "hat" above the variable denotes "estimate." Even if the process is not normal, this is still considered as a convenient form for variance estimates (e.g. ITTC (2017) Recommended Procedure 7.5-02-07-01.4).

3.6. Confidence interval of SSA

The estimate of SSA in Equation (11) is a random value. Randomness denotes that each time a quantity is estimated from another sample of the same general population, the value may be different. For simulated ship motions, an estimate of the ship motion parameter depends on a set of initial phases to generate irregular waves.

The confidence interval is a standard way to account for the randomness of an estimate. A probability that a true value is within a confidence interval is referred as confidence probability. A typical value for confidence probability is 0.95, which is recommended by MSC.1/Circ. 1627 (IMO, 2020) and mentioned in ITTC (2017) Recommended Procedure 7.5-02-07-01.4.

The technique for calculation of confidence interval of SSA is based on ITTC (2017) Recommended Procedure 7.5-02-07-01.4, while further background is available from Levine et al. (2017).

An estimate of the SSA is a deterministic function of a random argument $\widehat{V}_x$. The variance estimate $\widehat{V}_x$ is essentially a mean value of centered squares, so its distribution may be approximated as normal from the Central Limit Theorem. However, the variance is a positive value, while the normal distribution supports negative values. Usually, this is not a problem since the mean value of the estimate is sufficiently large, while the variance of the estimate is sufficiently small for the lower boundary of the confidence interval to not have negative support (denoted by a nonsensical value less than zero). If the assumption of normality is acceptable, the boundaries of the confidence interval based

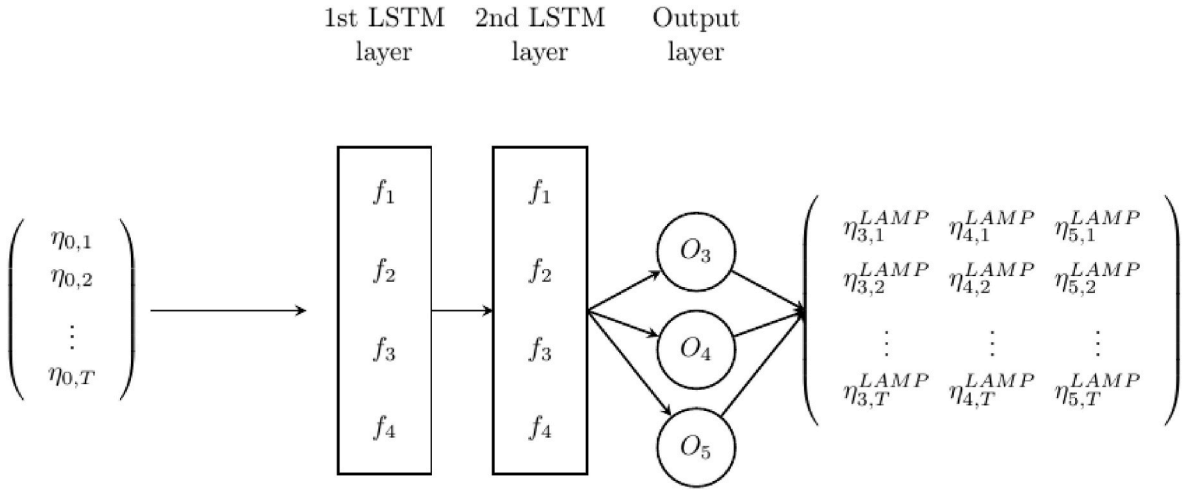

Fig. 5. LSTM-Waves architecture.

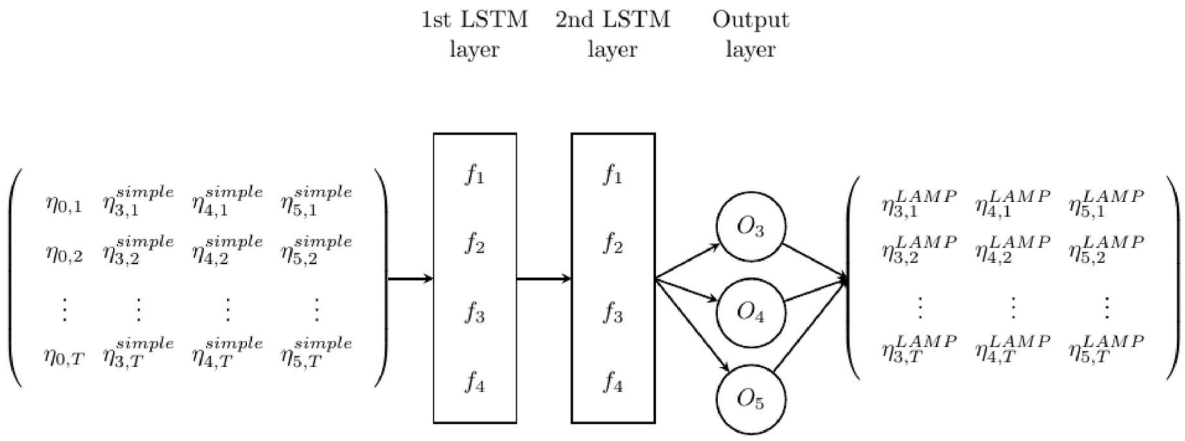

Fig. 6. LSTM-SimpleCode architecture.

Table 1
Parameters for LSTM architecture.

Parameter Definition	Variable
Input wave at time-step j	η_{oj}
Total number time steps	T
i^{th} degree-of-freedom (DOF) at time-step j	η_{ij}
k^{th} gate for LSTM layer	f_k
Number of LSTM units per layer	n
Output layer cell for DOF m	O_m

on the variance of the variance estimate $\widehat{V}(\widehat{V}_x)$ are:

$$\widehat{V}_x^{up} = \widehat{V}_x + Q_\beta \bullet \sqrt{\widehat{V}(\widehat{V}_x)};\ \widehat{V}_x^{low} = \widehat{V}_x + Q_\beta \bullet \sqrt{\widehat{V}(\widehat{V}_x)} \tag{12}$$

Q_B is the $\frac{(1+\beta)}{2}$ quantile of the standard normal distribution.

Since the function in the Longuet-Higgins (1984) model is monotonic and the problem is limited by the boundaries of the confidence interval, SSA can be calculated directly by applying Equation (11) to the boundaries of the variance estimate (Bickel and Doksum, 2001):

$$\widehat{SSA}_x^{up} = 2\sqrt{\widehat{V}_x^{up}};\ \widehat{SSA}_x^{low} = 2\sqrt{\widehat{V}_x^{low}} \tag{13}$$

The upper boundary of confidence interval of the SSA estimate of a motion parameter can inform an operator about the ship response.

4. Data-adaptive multi-fidelity model

4.1. Basic architecture

An objective of this study is to assess the initial feasibility of data-adaptive ship motion models for autonomous seakeeping. An emerging capability is data-adaptive tuning (or correction) of reduced-order model predictions based on training with higher fidelity data of ship motion responses. The intent of this data-adaptive approach is to improve the fidelity of a computationally-efficient reduced-order model.

In this framework, the higher fidelity target is LAMP and reduced-order model is SimpleCode. LAMP-2 is the version utilized in this study. LAMP-2 is based on a body-non-linear formulation for hydrostatic and Froude-Krylov forces, and body-linear for diffraction and radiation. For the given hull form geometry, wave conditions, and specified ship speeds and headings, LAMP simulations generate pseudo-random irregular waves and output 3-DOF motion response time-series, which serve as training and testing datasets. The equivalent input wave data are then applied to SimpleCode, which generates reduced-fidelity response time-series.

Two data-adaptive machine learning methods are considered. The first method is referred to as LSTM-Waves, and second as LSTM-SimpleCode. The basic architecture of the LSTM-Waves and LSTM-SimpleCode methods are in Figs. 5 and 6.

An additional fully connected linear output layer is incorporated after the two LSTM layers to parse the output into individual time-series channels of 3-DOF motions in terms of roll, pitch and heave. Definitions of the parameters are in Table 1.

LSTM-Waves method employs a network that is directly trained and tested with high-fidelity LAMP data. LSTM-Wave network is strictly data-driven and not physics-based. The single channel wave time-series are applied as input to the LSTM network. The output response time-series from the LSTM network are compared with the corresponding 3-DOF motion time-series from LAMP. Based on the difference between the LSTM and LAMP target response outputs, an adaptive learning rule is applied for the tuning of the LSTM network cells. During testing, the output responses of the trained LSTM-Wave network are compared with high-fidelity LAMP baseline data.

LSTM-SimpleCode method comprises two-stages with SimpleCode as the first stage and the LSTM network as the second. LSTM-SimpleCode is characterized as a hybrid approach with a physics-based reduced-order model followed by a data-adaptive stage. In this architecture, four time-series channels are applied as inputs to the LSTM network. The input channels encompass the 3-DOF motion responses from SimpleCode, and the corresponding input wave time-series data. The output response time-series from the two-stage LSTM-SimpleCode are compared to 3-DOF motion time-series target from LAMP.

Table 2
Particulars for the ONR tumblehome.

Particular	Value
Length (L_{BP})	154.00 m
Beam	22.0 m
Draft	5.5 m
Displacement	8730.0 t

4.2. Ship particulars

In this study, the hull form geometry and loading conditions are based on a model of the ONR Tumblehome configuration from the ONR

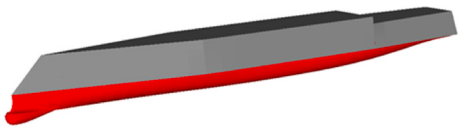

Fig. 7. Rendering of hull for ONR Tumblehome.

Table 3
Training values for hyperparameters.

Hyperparameter	Value
Time Resolution Factor	9
Hidden State Size	30
Number of LSTM Layers	2
Learning Rate	0.01

Topsides series (Bishop, et al., 2005). The particulars are listed in Table 2. A rendering of the hull form for the ONR Tumblehome model is in Fig. 7.

For the simulations, the model was free in the vertical plane for heave, roll and pitch, but constrained to constant course and speed in the horizontal plane for surge, sway and yaw.

4.3. LSTM configuration

The input time-series were arranged as $[n, N/\tau, \tau]$ arrays by number of inputs (n), number of points per realization (N), and time resolution factor (τ). Each LSTM layer consisted of a single LSTM cell with its own set of gates (f_1, f_2, f_3, f_4), distinct weights, and biases.

The hyperparameters were tuned with results from both head and beam sea configurations. Bi-directionality and dropout were found to increase computational expense with negligible gains in performance, and subsequently excluded from the training of LSTM-SimpleCode and LSTM-Waves. The training values for the hyperparameters are shown in Table 3.

A total of 30 realizations per parameter combination of LAMP data was generated with different sets of pseudo-random phases to ensure independence between realizations. Each realization was 30 min duration and 10 Hz sample rate. For the 30 LAMP simulations, 15 were targets for training, and 15 were for validation of the LSTM network. For training, the maximum number of epochs was 100 with an early stopping condition based on a 0.1% change in the best validation loss over 30 epochs.

The objective function for training was the mean-squared error (MSE) between LAMP and the LSTM output. The equation for MSE is given by:

$$MSE = \frac{1}{N}\sum_{I=1}^{N}\left(y_{LAMP}(t_i) - y_{LSTM}(t_i)\right)^2 \tag{14}$$

In this equation, LAMP time-series is represented by $y_{LAMP}(t)$, response time-series from LSTM network output is represented by $y_{LSTM}(t)$, number of samples in time-series (N), and time index t_i.

In training, individual LSTM networks were generated for each of the 91 speed-heading combinations. This was performed for LSTM-Waves and LSTM-SimpleCode networks separately, which resulted in a total of 182 individually trained LSTM network architectures. Alternatively, the LSTM networks could be trained with a more general approach covering a set of multiple speeds and headings.

4.4. Wave conditions and ship operating parameters

To assess the performance of both LSTM methods, LAMP and SimpleCode time-series were generated for a set of speed-heading combinations. Ship speeds ranged from 0 to 30 knots in 5 knot increments, and headings from 0 to 180° in 15° increments for a total of 91 speed-heading combinations.

Irregular unidirectional waves were generated based on the Longuet-Higgins (1984) model using a Bretschneider (1959) spectrum with significant wave height (H_s) of 4.0 m, and modal period (T_m) of 15.0 s.

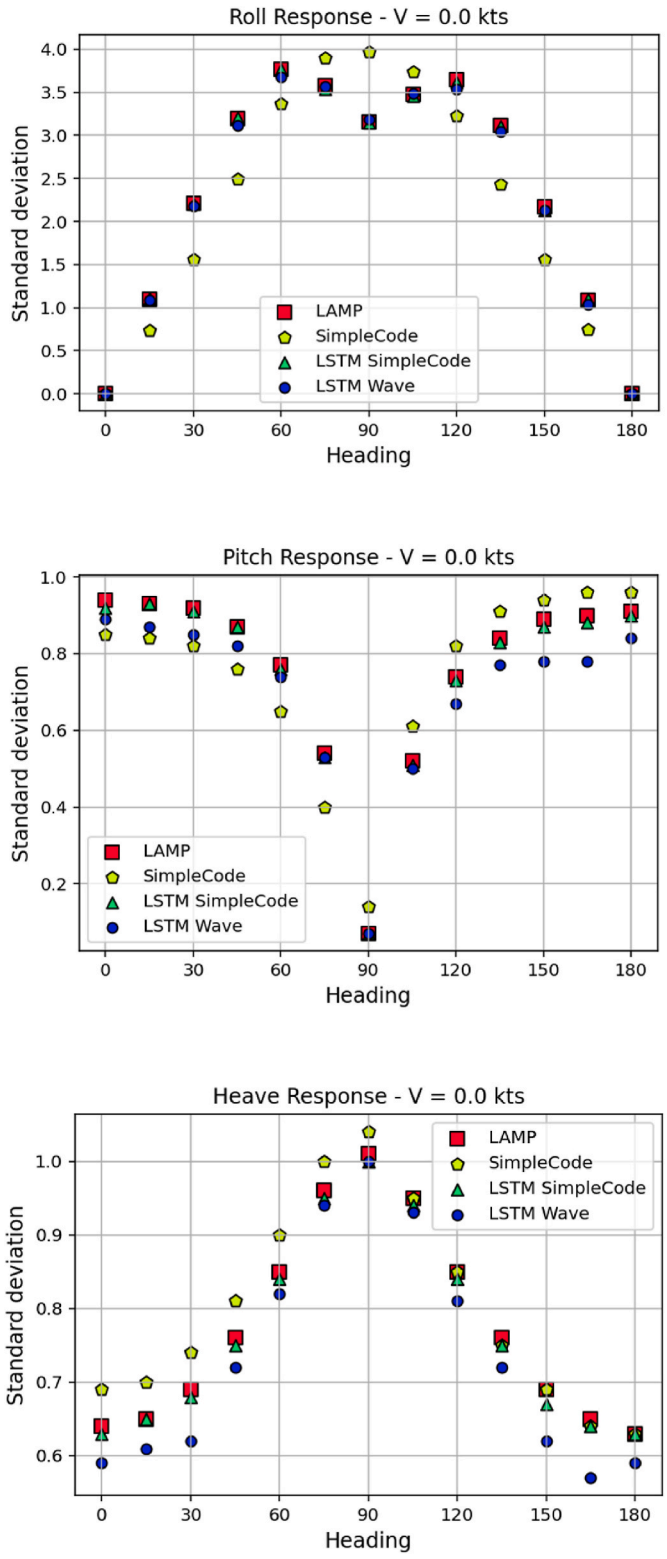

Fig. 8. Comparison of response levels versus heading for roll (top plot), pitch (middle), and heave (bottom) at speed = 0 knots.

4.5. Initial performance assessment

The performance of each LSTM-based method was assessed relative to LAMP and SimpleCode based on the comparison of the respective motion responses for heave, roll, and pitch. The average standard deviation was computed for the ensemble of each motion response type

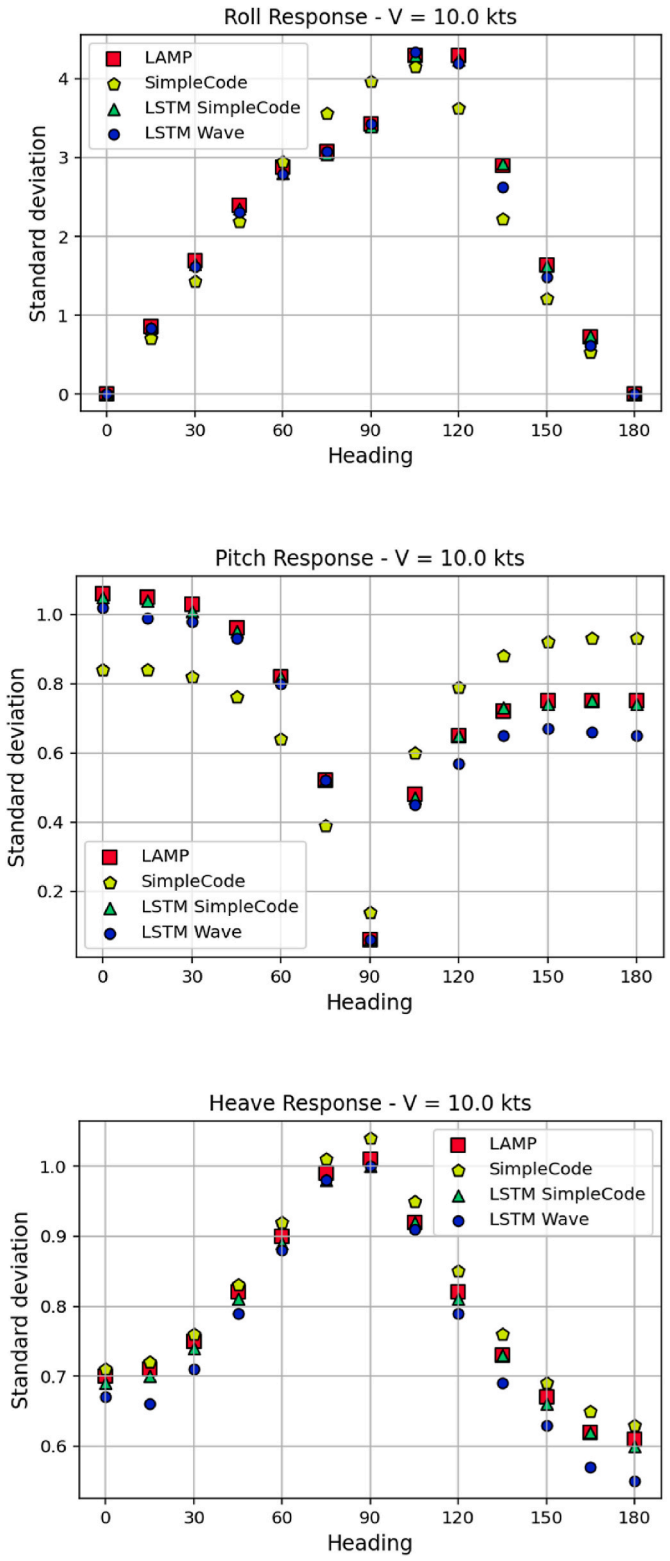

Fig. 9. Comparison of response levels versus heading for roll (top plot), pitch (middle), and heave (bottom) at speed = 10 knots.

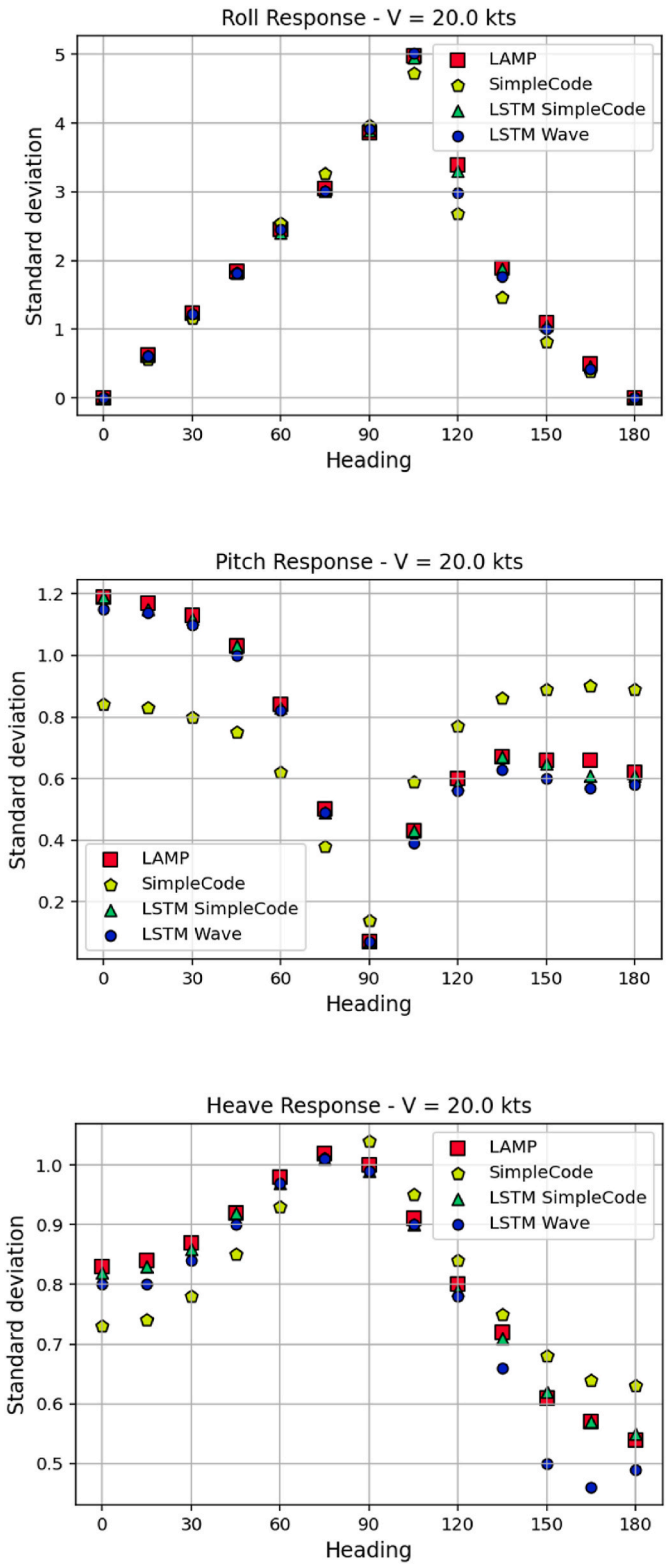

Fig. 10. Comparison of response levels versus heading for roll (top plot), pitch (middle), and heave (bottom) at speed = 20 knots.

and speed-heading combination, which provided the ship motion response statistics for this study.

For each speed-heading combination, 100 realizations of 3-DOF ship motion response time-series were generated by SimpleCode along with corresponding input wave time-series. As applicable, these ensembles were provided as inputs to the LSTM networks for the generation of the output realizations. Based on the computational efficiency of SimpleCode and wave generation, a larger number of realizations was readily achievable.

The average standard deviations of the realizations from SimpleCode, LSTM-Waves, and LSTM-SimpleCode were then compared respectively with the average standard deviations from LAMP.

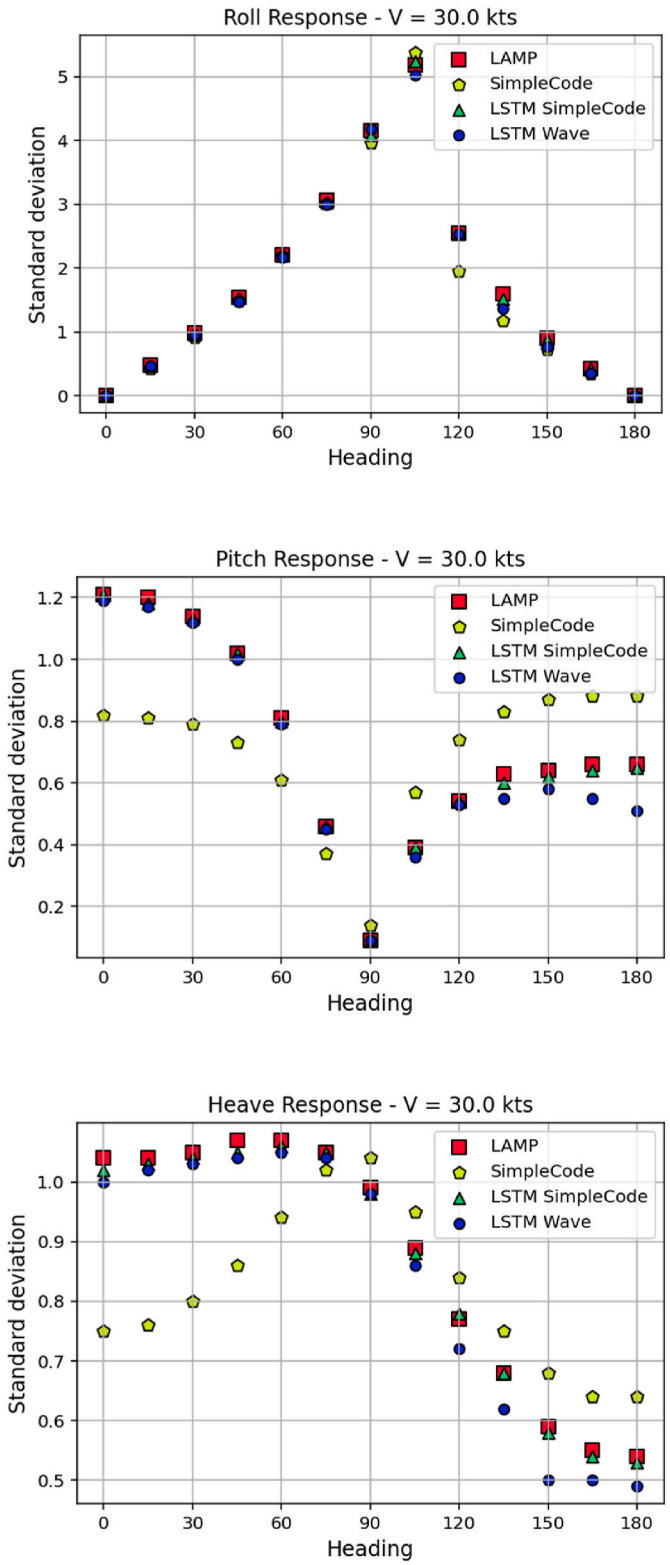

Fig. 11. Comparison of response levels versus heading for roll (top plot), pitch (middle), and heave (bottom) at speed = 30 knots.

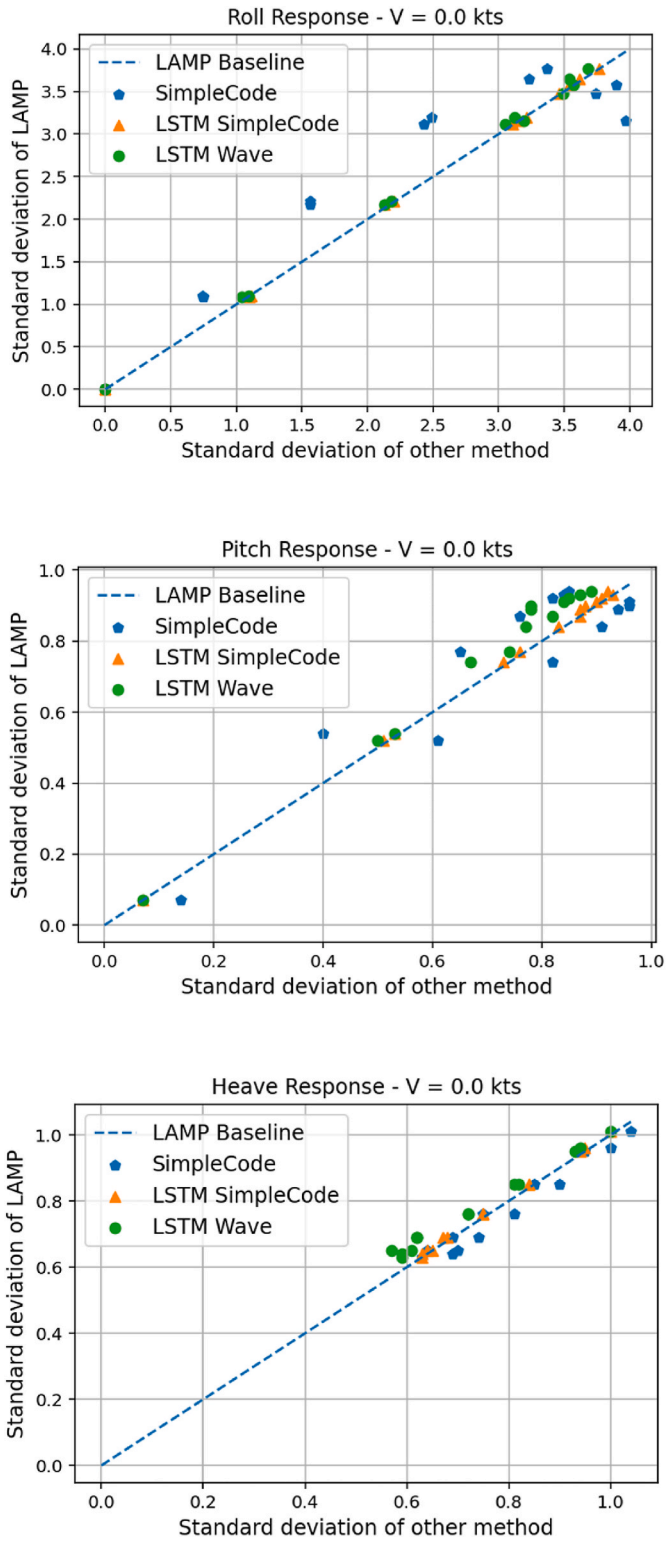

Fig. 12. Comparison of response levels versus LAMP baseline for roll (top plot), pitch (middle), and heave (bottom) at speed = 0 knots.

5. Results

This section presents the results of the comparative analysis of the ship motion statistics for LAMP, SimpleCode, LSTM-Waves, and LSTM-SimpleCode methods in terms of ship motion response plots and quantitative performance. As an illustrative example of seakeeping guidance, speed-heading polar plots of the 3-DOF ship motion responses from the LSTM-SimpleCode method are also provided.

For these comparisons, the standard deviation of the ship motion response from LAMP serves as the higher-fidelity target. Based on realizations from LAMP, the average standard deviation of the ensemble provides an estimate of the effective true standard deviation (Belenky, et al., 2015).

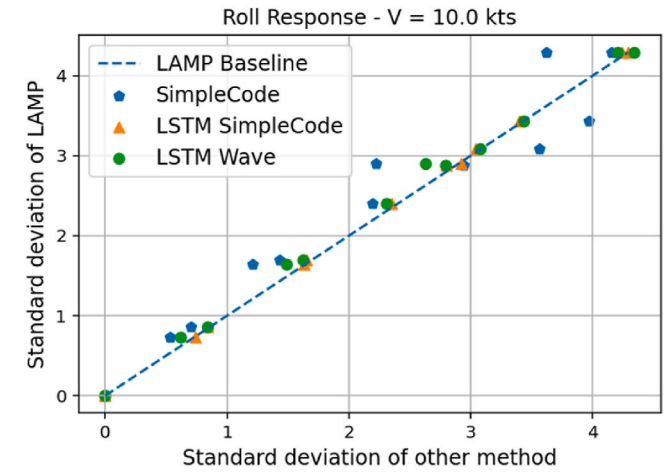

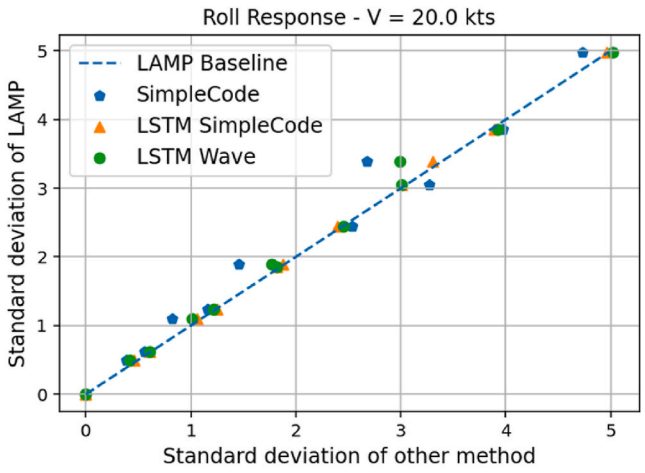

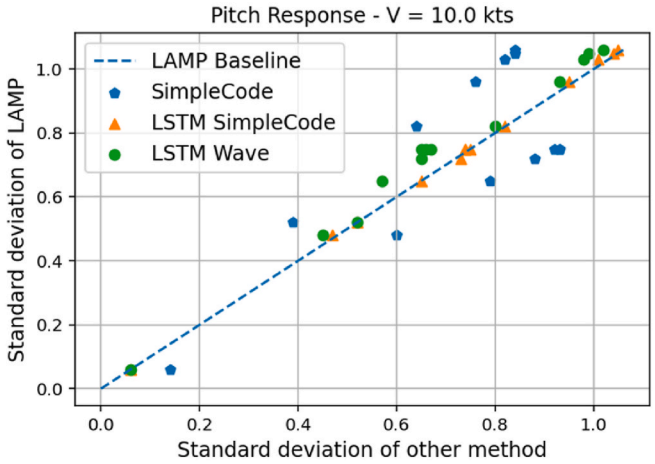

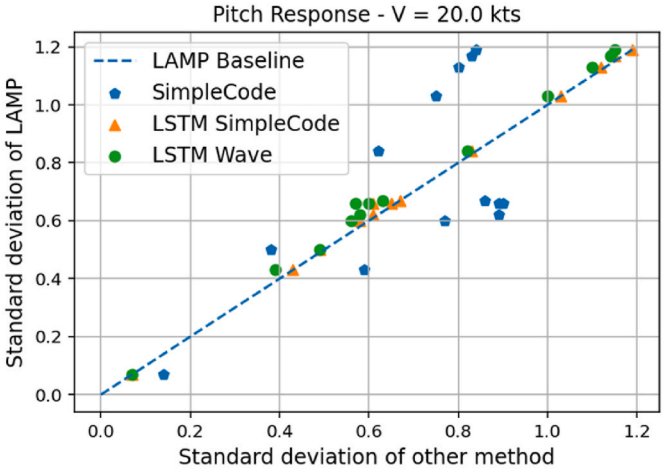

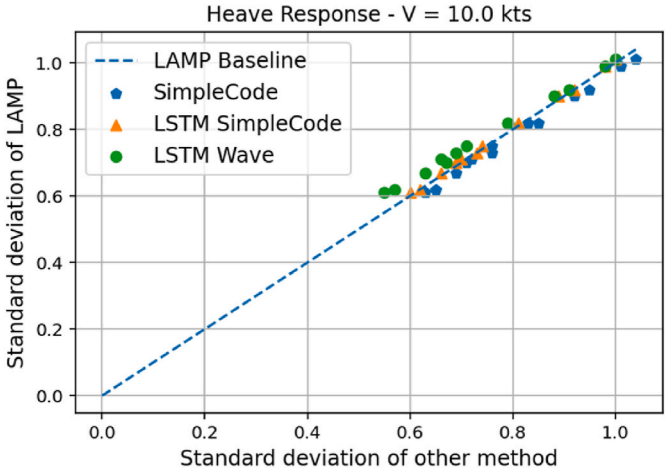

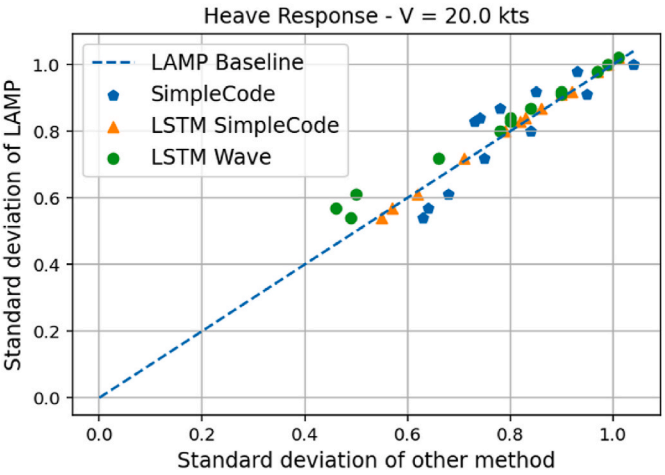

Fig. 13. Comparison of response levels versus LAMP baseline for roll (top plot), pitch (middle), and heave (bottom) at speed = 10 knots.

Fig. 14. Comparison of response levels versus LAMP baseline for roll (top plot), pitch (middle), and heave (bottom) at speed = 20 knots.

5.1. Response plot comparisons

Response plot comparisons are rendered in two ways. In the first view, response levels are plotted versus heading (in degrees) for roll, pitch and heave. Responses are provided for LAMP, SimpleCode, LSTM-Waves and LSTM-SimpleCode for speeds of 0, 10, 20 and 30 knots in Figs. 8–11, respectively. The heading convention for these and subsequent plots are head seas at 0°, following seas at 180°, and beam seas at 90 and 270°.

In the second view, response trend-line comparisons are plotted relative to the LAMP target (vertical axis) versus estimates for SimpleCode, LSTM-Waves, and LSTM-SimpleCode (horizontal axis), which are in Figs. 12–15.

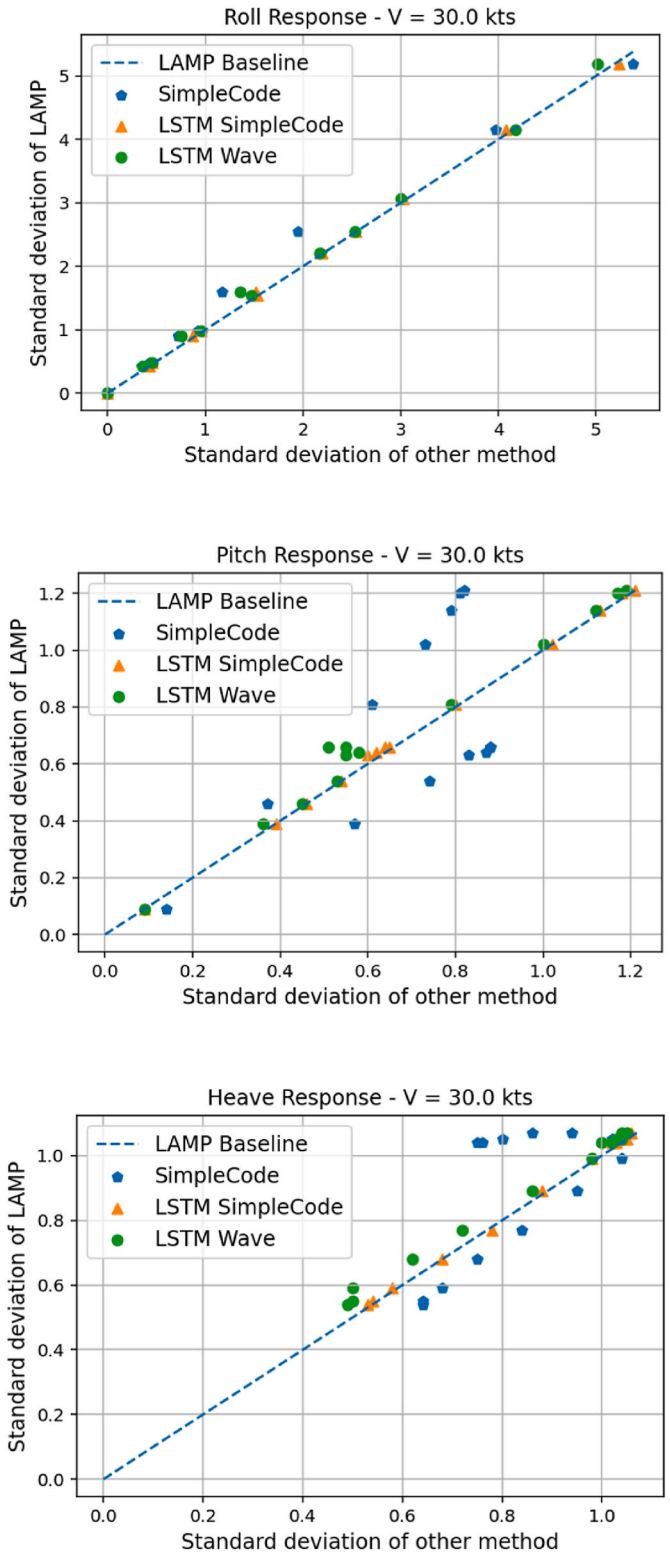

Fig. 15. Comparison of response levels versus LAMP baseline for roll (top plot), pitch (middle), and heave (bottom) at speed = 30 knots.

5.2. Metric-based comparison

As a quantitative metric for this assessment, R^2 scores for SimpleCode, LSTM-Waves, and LSTM-SimpleCode are computed with respect to the LAMP baseline at each speed across headings. This metric is computed as:

Table 4
R^2 scores comparison.

Motion	Speed (knots)	SimpleCode	LSTM-SimpleCode	LSTM-Waves
Heave	0.0	0.9299	0.9935	0.8685
	10.0	0.9697	0.9953	0.9217
	20.0	0.8116	0.9965	0.8890
	30.0	0.4052	0.9969	0.9566
Roll	0.0	0.8599	0.9998	0.9983
	10.0	0.9306	0.9994	0.9947
	20.0	0.9682	0.9994	0.9932
	30.0	0.9786	0.9994	0.9961
Pitch	0.0	0.8591	0.9975	0.9249
	10.0	0.5829	0.9988	0.9506
	20.0	0.4043	0.9970	0.9822
	30.0	0.3997	0.9983	0.9649

$$R^2 = 1.0 - \frac{MSE}{\sigma^2_{LAMP}} \tag{15}$$

σ^2_{LAMP} is the variance of the LAMP standard deviations, and *MSE* is defined in Equation (15). Resultant R^2 scores are summarized in Table 4.

Based on this comparisons, the LSTM-SimpleCode estimate most closely matched the LAMP target for each of the 3-DOF motions, headings, and speeds. In these cases, LSTM-SimpleCode R^2 values exceeded 0.99, and outperformed LSTM-Waves and SimpleCode. LSTM-Waves estimates closely matched the LAMP target for roll, but showed some differences for heave and pitch. SimpleCode had the lowest R^2 values particularly for pitch and heave at higher speeds.

5.3. Speed-heading polar plots

For operator guidance, speed-heading polar plots enable visualization of predicted ship motion responses to specified wave conditions. In seakeeping studies, response levels are typically computed as SSA. Fig. 16 illustrates the speed-heading polar plots for the 3-DOF ship motion responses predicted by the LSTM-SimpleCode method for the seaway condition with significant wave height of 4.0 m, and modal period of 15.0 s.

The plots are rendered from 0 to 360°; although, responses were only computed between 0 and 180°. Since this case involved a symmetrical hull in unidirectional seas, the responses have been mirrored.

In the polar plots, speeds and headings with the largest motion response can be identified by a human operator or automated detector. For this specific condition, the plots show the largest motion response for roll is around 105°, pitch at 0°, and heave at 75°. Generally, response levels at these headings are greater at higher speeds.

6. Conclusions

An objective of this study has to been to assess the potential feasibility of a data-adaptive multi-fidelity model for autonomous seakeeping. Data-adaptive tuning (or correction) of reduced-order model predictions have been implemented based on training with higher fidelity ship motion response data. From these initial results, this approach may provide a plausible means for improving the performance of a reduced-order model.

LSTM neural networks have been considered as part of a multi-fidelity approach for prediction of 3-DOF ship motion responses in waves. LSTM networks were trained and tested with LAMP simulations as a target, and SimpleCode simulations and wave time-series as inputs. LSTM networks improved the fidelity of SimpleCode seakeeping predictions relative to LAMP while retaining the computational efficiency of a reduced-order model.

LSTM-SimpleCode has been developed as a hybrid approach encompassing a physics-based model and data-adaptive stage. As a physics-based data-adaptive approach, LSTM-SimpleCode most closely

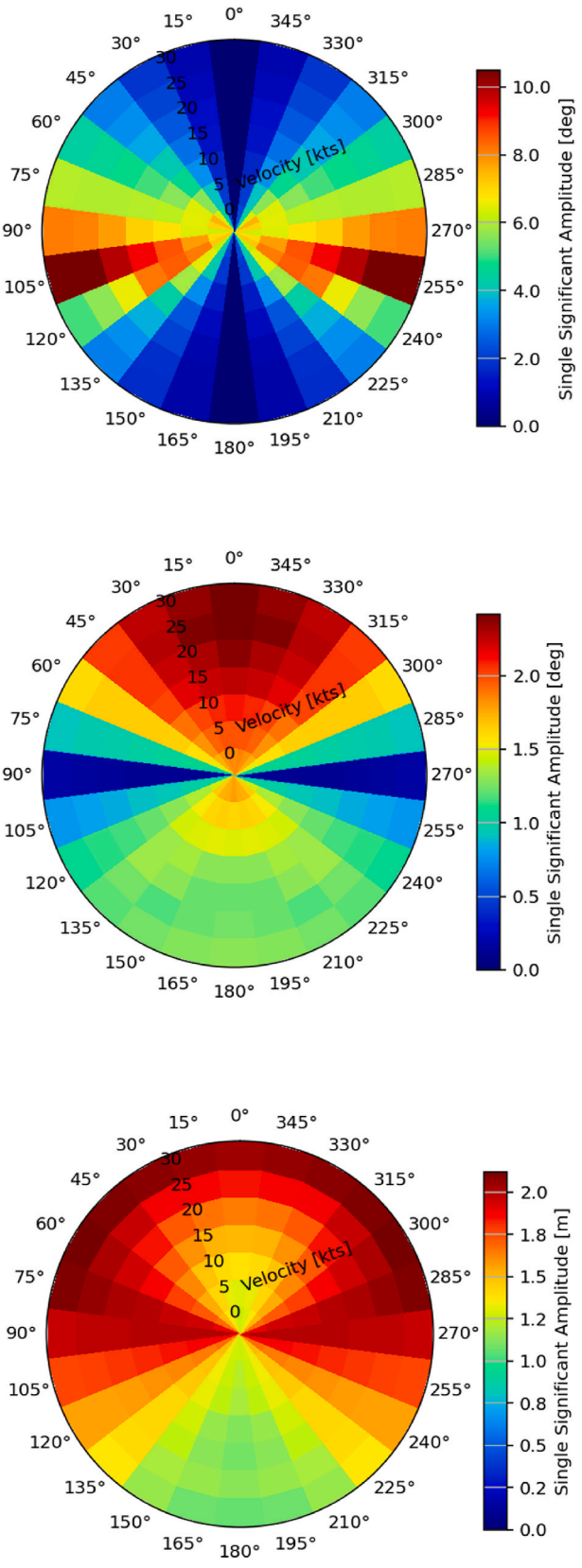

Fig. 16. Speed-heading SSA response polar plots from LSTM-SimpleCode method for roll (top plot), pitch (middle), and heave (bottom).

matched the LAMP target for each of the 3-DOF motions, headings, and speeds. In each case, LSTM-SimpleCode outperformed the strictly data-driven LSTM-Waves approach.

Based on the results of this study, LSTM-SimpleCode appears to be a suitable candidate for continued investigation and application including 6-DOF motions, structural loads, accelerations, and resistance.

For future investigation, selection of wave parameters for LSTM training based on historical climatological data could provide a more practical and efficient representation of potential seaway conditions, which are more likely to be encountered during real-world voyages.

CRediT authorship contribution statement

Michael D. Levine: Conceptualization, Methodology, Formal analysis, Writing – original draft, Writing – review & editing, Project administration. **Samuel J. Edwards:** Methodology, Software, Validation, Formal analysis, Data curation, Writing – original draft. **Dayne Howard:** Methodology, Writing – original draft. **Kenneth Weems:** Methodology, Software. **Themistoklis P. Sapsis:** Conceptualization. **Vladas Pipiras:** Formal analysis.

Declaration of competing interest

The authors declare that they have no known competing financial interests or personal relationships that could have appeared to influence the work reported in this paper.

Data availability

N/A.

Acknowledgements

The work described in this paper has been partially funded by the Office of Naval Research (ONR) under Dr. Woei-Min Lin.

References

ABS, 2019. Guide for the Assessment of Parametric Roll Resonance in the Design of Container Carriers. American Bureau of Shipping, Houston, Texas, USA.

Beck, R., Reed, A., 2001. Modern computational methods for ships in seaway. SNAME Transactions 109, 1–51, 2001.

Belenky, V., Yu, H., Weems, K.M., 2011. In: Neves, M.A.S., Belenky, V., de Kat, J.O., Spyrou, K., Umeda, N. (Eds.), "Numerical Procedures and Practical Experience of Assessment of Parametric Roll of Container Carriers," Chapter 16 of Contemporary Ideas on Ship Stability. Springer, pp. 295–396. ISBN 978-94-007-1481-6.

Belenky, V., Pipiras, V., Weems, K., 2015. Procedure for probabilistic evaluation of large amplitude roll motions. In: Proceedings of the 12th International Conference on the Stability of Ships and Ocean Vehicles. Glasgow, UK.

Belknap, W., Reed, A., 2019. TEMPEST—a new computationally efficient dynamic stability prediction tool. In: Contemporary Ideas on Ship Stability. Risk of Capsizing. Springer International Publishing, pp. 3–21.

Bertram, V., 2011. Practical Ship Hydrodynamics, second ed. Butterworth-Heinemann. ISBN 978-0080971506, 2011.

Bickel, P. J., and Doksum, K. A., Mathematical Statistics: Basic Ideas and Selected Topics, Vol. vol. 1. Person Prentice Hall.

Bishop, R.C., Belknap, W., Turner, C., Simon, B., Kim, J.H., 2005. "Parametric Investigation on the Influence of GM, Roll Damping, and Above-Water Form on the Roll Response of Model 5613". Naval Surface Warfare Center Carderock Division, West Bethesda, Maryland, USA. Technical Report NSWCCD-50-TR-2005/027.

Bretschneider, C.L., 1959. Wave variability and wave spectra for wind-generated gravity waves. In: Technical Memorandum 118. U.S. Army Beach Erosion Board, Washington, DC.

Dong, Y., Frangopol, D., Sabatino, S., 2016. A decision support system for mission-based ship routing considering multiple performance Criteria. Reliab. Eng. Syst. Saf. 150, 190–201.

France, W.M., Levadou, M., Treakle, T.W., Paulling, J.R., Michel, K., Moore, C., 2003. An investigation of head-sea parametric rolling and its influence on container lashing systems. Mar. Technol. 40 (1), 1–19.

Hochreiter, S., Schmidhuber, J., 1997. Long short-term memory. Neural Comput. 9 (11), 1735–1780.

IACS, 2001. Recommendation No. 34 Standard Wave Data. International Association of Classification Societies Recommendation, London, UK.

IMO, 2020. "Interim Guidelines on the Second Generation Intact Stability Criteria," MCS.1/Circ. 1627. International Maritime Organization, London, UK.
IMO, 2007. Revised Guidance to the Master for Avoiding Dangerous Situations in Adverse Weather and Sea Conditions. International Maritime Organization, London, UK. MCS.1/Circ. 1228.
IMO, 1995. "Guidance to the Master for Avoiding Dangerous Situations in Following and Quartering Seas". International Maritime Organization, London, UK. MSC/Circ. 707.
ITTC, 2017. Single significant amplitude and confidence intervals for stochastic processes. In: Recommended Procedure 7.5-02-07-01.4, 28th International Towing Tank Conference.
ITTC, 2021. Estimation of roll damping. In: Recommended Procedure 7.5-02-07-04.5, 29th International Towing Tank Conference.
Levadou, M., van't Veer, R., 2006. Parametric roll and ship design. In: Proceedings of the 9th International Conference on Stability of Ships and Ocean Vehicles (STAB 2006), vol. 1, pp. 191–206. Rio-de-Janeiro, Brazil.
Levine, M.D., Belenky, V., Weems, K., 2017. Statistical Uncertainty Techniques for Analysis of Simulation and Model Test Data," 30th American Towing Tank Conference. Naval Surface Warfare Center, Carderock Division, West Bethesda, Maryland, USA.
Lin, W., Yue, D., 1990. Numerical solutions for large amplitude ship motions in the time-domain. In: Proceedings of the 18th Symposium on Naval Hydrodynamics. Ann Arbor, Michigan, USA.
Longuet-Higgins, M.S., 1984. Statistical properties of wave groups in a random sea state. Phil. Trans. Roy. Soc. Lond.: Math. Phys. Eng. Sci. 312 (1521), 219–250.
Nielsen, U.D., Jensen, J.J., 2011. A novel approach for navigational guidance using onboard monitoring systems. Ocean Eng. 38, 444–455.
Nielsen, U.D., Lajic, Z., Jensen, J.J., 2012. Towards Fault-Tolerant Decision Support Systems for Ship Operator Guidance, vol. 104. Reliability Engineering & System Safety, pp. 1–14.
Pipiras, P., Belenky, V., Weems, K., Brown, B., Frommer, A., Ouimette, G., 2021. Calibrating multifidelity ship motion codes through regression. In: Proceedings of the 1st International Conference on the Stability and Safety of Ships and Ocean Vehicles. Glasgow, UK.
Qiao, D., Li, P., Ma, G., Qi, X., Yan, J., Ning, D., Li, B., 2021. Realtime prediction of dynamic mooring lines responses with LSTM neural network model. Ocean Eng. 219 (1).
Shin, Y.S., Belenky, V., Lin, W.M., Weems, K.M., 2003. Nonlinear time domain simulation technology for seakeeping and wave-load analysis for modern ship design. SNAME Transactions 111, 557–578.
Silva, K.M., Knight, B.G., Maki, K.J., 2022. Numerical prediction of extreme roll of a free-running ship with computational fluid dynamics and neural networks. In: Proceedings of the 34th Symposium of Naval Hydrodynamics. Washington, D.C.
Shin, Y.S., Belenky, V.L., Paulling, J.R., Weems, K.M., Lin, W.M., 2004. Criteria for parametric roll of large containerships in longitudinal seas. SNAME Transactions 112, 14–47.
Smith, T.C., 2019. In: Belenky, V., Neves, M., Spyrou, K., Umeda, N., van Walree, F. (Eds.), "Validation Approach for Statistical Extrapolation," Chapter 34 of Contemporary Ideas on Ship Stability. Risk of Capsizing. Springer, pp. 573–589. ISBN 978-3-030-00514-6.
Weems, K. M., and Wundrow, D., 2, 013"Hybrid models for the fast time-domain simulation of stability failures in irregular waves with volume based calculations for froude-krylov and hydrostatic forces," Proceedings of the 13th International Ship Stability Workshop, Brest, France.
Weems, K., Belenky, V., 2018. Extended fast ship motion simulations for stability failures in irregular seas. In: Proceedings of the 13th International on Stability of Ships and Ocean Vehicles. Kobe, Japan.
Weems, K., Belenky, V., Spyrou, K., Aram, S., Silva, K., 2020. Towards numerical estimation of probability of capsizing caused by broaching-to. In: Proceeding of the 33rd Symposium of Naval Hydrodynamics. Osaka, Japan.
Xu, W., Maki, K.J., Silva, K.M., 2021. A data-driven model for nonlinear marine dynamics. Ocean Eng. 236 (9).